Christian Marinus Huber*, Andreas Benedikter, Helmut Ermert, Martin Vossiek, Ingrid Ullmann, and Stefan Lyer

Passive Acoustic Mapping of Cavitation in Heterogeneous Speed of Sound Distributions using the Fast Marching Method

https://doi.org/10.1515/cdbme-2025-0183

Abstract: Passive Acoustic Mapping (PAM) is a technique used to localize cavitation events in biomedical applications such as targeted drug delivery, histotripsy, and lithotripsy. Accurate cavitation mapping is essential for optimizing therapeutic efficacy and safety. However, conventional PAM assumes a homogeneous speed of sound within tissue, which does not reflect the heterogeneous acoustic properties of biological media. In this work, we introduce the Fast Marching Method (FMM) to PAM for accurately computing time delays in arbitrary speed of sound distributions. We evaluate the proposed approach through simulations, demonstrating its potential for improved cavitation mapping in realistic tissue environments.

Keywords: Ultrasound, Numerical Method, Travel time Computation, Biomedical Application, Passive Imaging

1 Introduction

Ultrasound-induced cavitation plays an important role in various biomedical applications, including localized drug delivery [1], histotripsy [2], and lithotripsy [3]. A significant area of research is the use of focused ultrasound (FUS) to induce cavitation for blood-brain barrier (BBB) opening [4]. In this context, the heterogeneous tissue environment introduces sound speed variations, requiring aberration correction methods for both ultrasound propagation and subsequent image formation.

To monitor cavitation events, ultrasound-based Passive

*Corresponding author: Christian Marinus Huber, Department of Otorhinolaryngology, Head and Neck Surgery, Section of Experimental Oncology and Nanomedicine (SEON), Professorship for Al-Controlled Nanomaterials (KINAM), Universitätsklinikum Erlangen, Germany; Institute of Microwaves and Photonics (LHFT), Friedrich-Alexander-Universität Erlangen-Nürnberg, e-mail: Christian.ch.huber@fau.de

Andreas Benedikter, Microwaves and Radar Institute, German Aerospace Center (DLR), Oberpfaffenhofen, Germany Martin Vossiek, Ingrid Ullmann, LHFT.

Friedrich-Alexander-Universität Erlangen-Nürnberg, Erlangen, Germany

Helmut Ermert, Stefan Lyer, Department of Otorhinolaryngology, Head and Neck Surgery, SEON, KINAM, Universitätsklinikum Erlangen, Germany

Acoustic Mapping (PAM) [5] is commonly employed. This technique utilizes an ultrasound array to passively receive acoustic emissions from cavitation events, followed by beamforming in either the time or frequency domain [6] to reconstruct the cavitation source map. Common beamforming approaches include Delay-And-Sum (DAS) [5], higher-order Delay-Multiply-And-Sum (DMAS) [7, 8], the Robust Capon Beamformer [9], and the Angular Spectrum Method (ASM) [10]. However, most of these methods assume - in their standard form - a homogeneous speed of sound distribution, with the exception of the adapted ASM.

In this work, we introduce the Fast Marching Method (FMM) [11] to compute time delays for time-domain PAM methods (time exposure acoustics PAM (TEA-PAM)). FMM provides a flexible and efficient solution for handling arbitrary speed of sound distributions and can be easily integrated into various PAM techniques, unlike the ASM, which is limited to a specific approach. Originally developed for seismic tomography (as PAM [12]), FMM has also been applied in other fields such as radar inversion [13]. In this contribution, the enhanced Multistencil FMM (MSFMM) [14] is utilized with TEA-PAM.

2 Methods and Materials

2.1 Passive Acoustic Mapping

The passively received radiofrequency (RF) data $s_n(t)$ for the n-th transducer array element, located at $(x_n, z_n) = (x_n, 0)$ within an array of N elements is utilized in a DAS scheme

$$q(\mathbf{x},t) = \frac{1}{N\alpha} \sum_{n=1}^{N} s_n(t + \tau_n(\mathbf{x}))$$
 (1)

to compute the source strenght q, with α as the piezoelectric coefficient. $\tau_n(\mathbf{x}) = \sqrt{z^2 + (x_n - x)^2}/c$ is the time delay from point $\mathbf{x} = (x, z)$ with assumed speed of sound c (see Fig. 2). After beamforming, the TEA operation is used to generate the cavitation map of source intensity using

$$I(\mathbf{x}) = \frac{1}{\rho_0 c} \sum_{m=1}^{M} q(\mathbf{x}, m \cdot \Delta t)^2, \tag{2}$$

where ρ_0 is the density of the propagation medium, Δt is the time discretization of the RF data and $M \cdot \Delta t = T$ denotes the total time period.

The utilized parameter c and ρ_0 are assumed to be distributed homogeneously in the propagation medium. In real tissue this is not the case and c and ρ are dependent on position $c \to c(\mathbf{x}), \rho_0 \to \rho_0(\mathbf{x})$. In this contribution, the speed of sound distribution dependency of Eq. (1) for the time delay is evaluated using the MSFMM. The combination of PAM with the MSFMM is called FMM-PAM.

2.2 Fast Marching Method

The FMM is an iterative, grid-based numerical solver for the Eikonal equation

$$|\nabla t(x,y,z)| = \frac{1}{c(x,y,z)},\tag{3}$$

where t(x,y,z) represents the travel time (TT) wavefront, and c(x,y,z) denotes the spatially varying speed of sound. Equation 3 is a high-frequency approximation of the wave equation, describing wavefront propagation in heterogeneous media.

In the FMM framework, the computational grid is classified into three categories: alive, narrow band and far points. Alive points correspond to grid nodes with finalized TT values from previous iterations. Narrow-band points are neighboring nodes of the alive set with trial TT values, whereas far points compromise all remaining nodes yet to be processed.

The initialization step assigns the source node a travel time of t=0 s and designates it as alive. The TT values of adjacent grid nodes are then estimated using a first-order approximation using $t=\frac{\Delta}{c}$, where Δ represents the grid spacing. These computed TT values are placed in the narrow-band set. Subsequently, the narrow-band node with the smallest TT is promoted to the alive set, and its neighboring nodes undergo TT recomputation before being added to the narrow band. This process iterates until all points are classified as alive.

Various FMM variants exist for TT estimation, including the standard FMM, higher-order FMM, diagonal FMM, and MSFMM, among others. The following discussion focuses on their application in two-dimensional (2D) domains, although these methods extend naturally to three-dimensional (3D) problems.

To implement MSFMM, uniform grid spacing across all dimensions is needed, i.e., $(\Delta = \Delta_x = \Delta_z)$. All FMM approaches aim to numerically solve the Eikonal equation in the form

$$\frac{1}{c(i,j)^2} = \sum_{v=1}^{2} \max \{ F \cdot (t(i,j) - t_v), 0 \}^2, \tag{4}$$

where F depends on the approximation order: $F=1/\Delta$ for first-order accuracy and $F=3/(2\Delta)$ for second-order approximation. The indices (i,j) denote discretized grid nodes in a 2D domain. Equation (4) can be solved using the quadratic formula

$$t(i,j) = \frac{-b \pm \sqrt{b^2 - 4ac}}{2a},\tag{5}$$

where a, b and c are the quadratic, linear, and constant coefficients, respectively.

To integrate diagonal contributions in MSFMM, the computational grid is rotated such that diagonal nodes are treated as standard ones, after which TT values are computed using the same iterative procedure. The modified grid spacing along the diagonal is given by $\Delta_{\rm rot,1}=\sqrt{2}\Delta.$

For first order FMM, the travel times in Equation 4 are determined as

$$t_1 = \min\{t_{i-1,j}, t_{i+1,j}\}; \quad t_2 = \min\{t_{i,j-1}, t_{i,j+1}\}.$$
 (6)

For second-order accuracy, they are refined as

$$t_{1} = \min \left\{ \frac{4 \cdot t_{i-1,j} - t_{i-2,j}}{3}, \frac{4 \cdot t_{i+1,j} - t_{i+2,j}}{3} \right\},$$

$$t_{2} = \min \left\{ \frac{4 \cdot t_{i,j-1} - t_{i,j-2}}{3}, \frac{4 \cdot t_{i,j+1} - t_{i,j+2}}{3} \right\}.$$
(7)

To further enhance the accuracy of MSFMM, standard and diagonal directional contributions can be combined as

$$t(i,j) = \frac{-(b+b') + \sqrt{(b+b')^2 - 4(a+a')(c+c')}}{2(a+a')}, \quad (8)$$

where a, b, c are the coefficients of the regular grid and a', b', c' the coefficients in the diagonal direction. For PAM, the TT wavefront are computed for the image region for each array element. For the following simulation, only one TT wavefront from the source position to all array elements is computed (see Figure 1 Travel time Wavefront)

2.3 In Silico Evaluation

For the evaluation, RF data is simulated for a single cavitation bubble located at $\mathbf{x}_b = (0, 50 \text{ mm})$ using the model proposed in [15]

$$s_n(t) = \sum_{k=-20}^{20} \frac{p_k}{d_n(\mathbf{x}_b)} \exp\left\{\frac{-|t - kT_0 - \phi_k - \tau_n(\mathbf{x}_b)|}{\theta_k}\right\},\tag{9}$$

where $T_0 = 1/f_0$ with $f_0 = 835$ kHz representing the pulse period, and k is a counter for the current pulse period. The parameters p_k (peak acoustic pressure), ϕ_k (phase offset), and θ_k

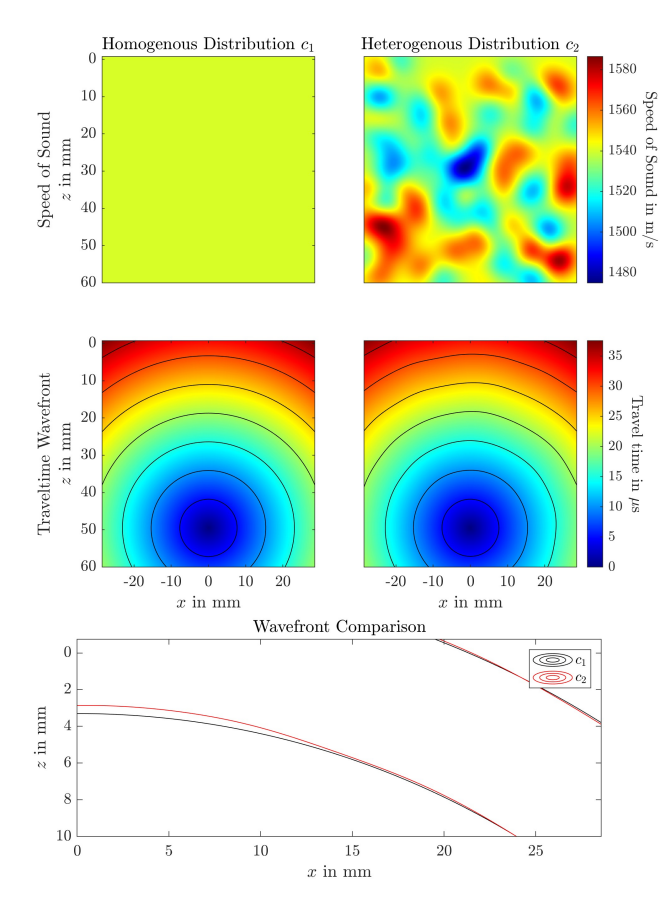


Fig. 1: Utilized speed of sound distributions c_1 (homogeneous) and c_2 (heterogeneous) and their corresponding travel time wavefront for a source at (x,z)=(0,50) mm. The bottom plot shows a zoomed in area to compare the wavefronts.

(time constant) are modeled as normally distributed random variables: $p_k \sim \mathcal{N}\{3 \text{ MPa}, 10 \text{ kPa}\}, \ \phi_k \sim \mathcal{N}\{1 \text{ µs}, 14 \text{ ns}\},$ and $\theta_k \sim \mathcal{N}\{2 \text{ ns}, 0.5 \text{ ns}\},$ where $\mathcal{N}\{\mu, \sigma\}$ denotes a normal distribution with mean μ and standard deviation σ .

Two test cases are considered for evaluation. In the first case, a homogeneous speed of sound $c_1=c_0=1540$ m/s is assumed, representing the conventional approach. This test case serves to validate the performance of the FMM in a standard scenario, in comparison with TEA-PAM. In the second case, a heterogeneous speed of sound distribution c_2 is introduced (see Fig. 1). For this case, Eq. (9) is modified such that $\tau_n(\mathbf{x}_b)=t_{\rm FMM}, n(\mathbf{x}_b)$ and $d_n(\mathbf{x}_b)=t_{\rm FMM}, n(\mathbf{x}_b) \cdot c_0$, incorporating the FMM-based travel-time corrections.

The simulation setup is illustrated in Fig. 2. The transducer array consists of N=128 elements, with positions defined as $x_n=(-19.05+w_{\rm pitch}\cdot(n-1))$ for $n\in\mathbb{N},1\leq n\leq N$ and $w_{\rm pitch}=0.3$ mm.

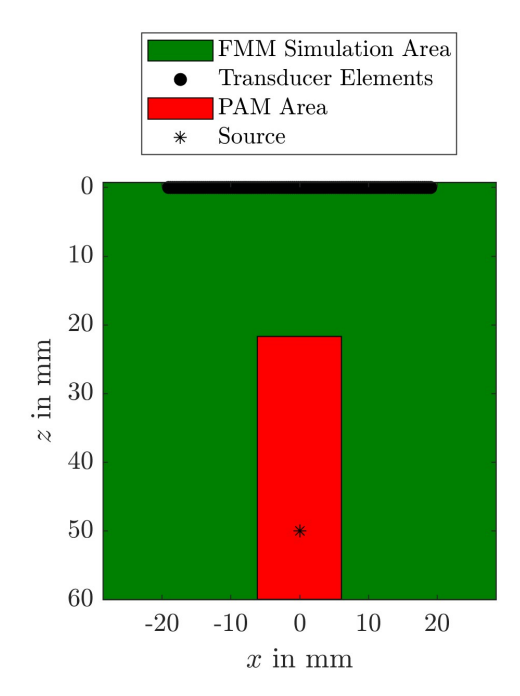


Fig. 2: Setup used in the simulation.

3 Results and Discussion

The simulation results using the MSFMM to compute the time delays from the source position $\mathbf{x}_b = (0,50)$ mm are presented in Fig. 1 for both the homogeneous (c_1) and heterogeneous (c_2) speed of sound distributions. The computed TT wavefronts for both cases exhibited a high degree of similarity, with only minor deviations, as illustrated in the last plot of Fig. 1. However, these small differences significantly impacted source reconstruction, as demonstrated in Fig. 3, which compares the results of standard PAM and FMM-PAM for both speed of sound distributions.

For the homogeneous case, both standard PAM and FMM-PAM yielded identical source reconstructions at $\mathbf{x}_{PAM,1}=(0,49.43)$ mm and $\mathbf{x}_{FMM-PAM,1}=(0,49.43)$ mm. This agreement was expected and confirmed the accuracy of the TT wavefronts computed using the FMM. However, for the heterogeneous distribution, the standard PAM method incorrectly reconstructed the source at $\mathbf{x}_{PAM,2}=(0.53,41.55)$ mm, accompanied by strong artifacts. In contrast, FMM-PAM accurately reconstructed the source at the same location as before, $\mathbf{x}_{FMM-PAM,2}=(0,49.43)$ mm, demonstrating the potential of this approach for accurate passive acoustic mapping in heterogeneous media.

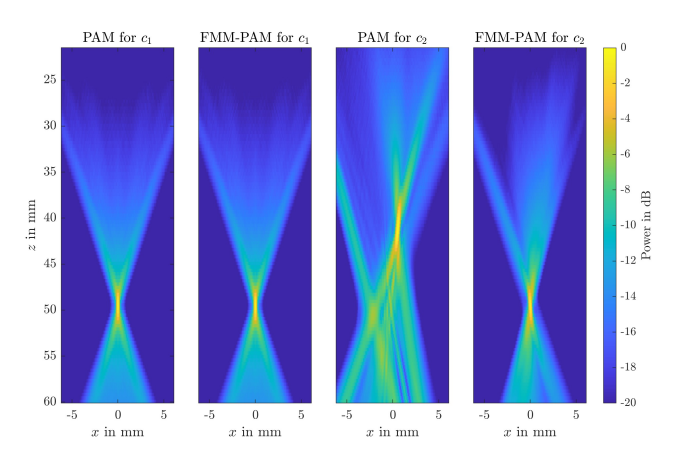


Fig. 3: Results for passive acoustic mapping (PAM) in combination with the multistencil Fast Marching Methog (FMM-PAM) for a simulated source at (x,z)=(0,50) mm.

4 Conclusion

In this work, we introduced the Fast Marching Method for passive acoustic mapping in arbitrary speed of sound distributions. This approach enables aberration correction, leading to improved source reconstruction. Using a standard simulation, we demonstrated that while the standard TEA-PAM method incorrectly mapped the source position in a heterogeneous speed of sound distribution, the proposed FMM-PAM method accurately reconstructed it.

However, it is important to note that this improvement is only achievable if the speed of sound distribution is precisely known in advance. This assumption is rarely met in practice. Future studies will focus on reconstructing speed of sound maps using travel-time inversion, which can then be integrated into FMM-PAM. Ultimately, this method aims to serve as an ultrasound-based technique for mapping ultrasound-induced cavitation events during magnetic drug targeting [16–18].

Author Statement

Research funding: The authors gratefully acknowledge the financial support of the Deutsche Forschungsgemeinschaft (DFG) - project number 452821018 and the Julitta und Richard Müller Stiftung. Conflict of interest: Authors state no conflict of interest.

References

[1] Moom Sinn Aw, et al. The progressive role of acoustic cavitation for non-invasive therapies, contrast imaging and blood-tumor permeability enhancement. Expert opinion on drug delivery, 13(10):1383–1396, 2016.

- [2] Yufeng Zhou and Xiaotong Wang. Effect of pulse duration and pulse repetition frequency of cavitation histotripsy on erosion at the surface of soft material. *Ultrasonics*, 84:296– 309. 2018.
- [3] Morteza Ghorbani, et al. Review on lithotripsy and cavitation in urinary stone therapy. *IEEE reviews in biomedical* engineering, 9:264–283, 2016.
- [4] Tao Sun, et al. Acoustic cavitation-based monitoring of the reversibility and permeability of ultrasound-induced bloodbrain barrier opening. *Physics in medicine and biology*, 60(23):9079–9094, 2015.
- [5] Miklós Gyöngy and Constantin-C Coussios. Passive spatial mapping of inertial cavitation during hifu exposure. *IEEE* transactions on bio-medical engineering, 57(1):48–56, 2010.
- [6] Kevin J. Haworth, et al. Quantitative frequency-domain passive cavitation imaging. *IEEE transactions on ultrasonics*, ferroelectrics, and frequency control, 64(1):177–191, 2017.
- [7] Shukuan Lu, et al. Delay multiply and sum beamforming method applied to enhance linear-array passive acoustic mapping of ultrasound cavitation. *Medical physics*, 46(10):4441–4454, 2019.
- [8] Christian Marinus Huber, et al. Passive Cavitation Mapping for Biomedical Applications Using Higher Order Delay Multiply and Sum Beamformer with Linear Complexity. 2024.
- [9] Christian Coviello, et al. Passive acoustic mapping utilizing optimal beamforming in ultrasound therapy monitoring. The Journal of the Acoustical Society of America, 137(5):2573– 2585, 2015.
- [10] Scott Schoen and Costas D. Arvanitis. Heterogeneous angular spectrum method for trans-skull imaging and focusing. IEEE transactions on medical imaging, 39(5):1605–1614, 2020
- [11] J. A. Sethian. Fast marching methods. SIAM Review, 41(2):199–235, 1999.
- [12] Stephen J. Norton, et al. Passive imaging of underground acoustic sources. *The Journal of the Acoustical Society of America*, 119(5):2840–2847, 2006.
- [13] Christian Marinus Huber, et al. Radar travel time tomography for subsurface ice exploration at saturn's moon enceladus. In 2021 18th European Radar Conference (EuRAD), pages 433–436. IEEE, 2022.
- [14] M. Sabry Hassouna and A. A. Farag. Multi-stencils fast marching methods: a highly accurate solution to the eikonal equation on cartesian domains. *IEEE transactions on pattern* analysis and machine intelligence, 29(9):1563–1574, 2007.
- [15] K. Vokurka. A method for evaluating experimental data in bubble dynamics studies. *Czechoslovak Journal of Physics*, 36(5):600–615, 1986.
- [16] Christian Huber, et al. Ultrasound-mediated cavitation of magnetic nanoparticles for drug delivery applications. Current Directions in Biomedical Engineering, 8(2):568–571, 2022.
- [17] Christian Marinus Huber, et al. Ultrasound-induced stable and inertial cavitation of magnetic nanoparticles for drug delivery applications. *Current Directions in Biomedical Engi*neering, 10(4):328–331, 2024.
- [18] Christian Marinus Huber, et al. A review on ultrasound-based methods to image the distribution of magnetic nanoparticles in biomedical applications. *Ultrasound in medicine & biology*, 51(2):210–234, 2025.